

Importance of the chromophore orientation to the ligand-to-metal energy transfer in lanthanide complexes with pendant-arm fitted cyclen derivatives †

Gaël Zucchi, Rosario Scopelliti and Jean-Claude G. Bünzli

Institute of Inorganic and Analytical Chemistry, University of Lausanne, CH-1015 Lausanne, Switzerland. E-mail: Jean-Claude.Bunzli@icma.unil.ch

Received 9th February 2001, Accepted 11th May 2001

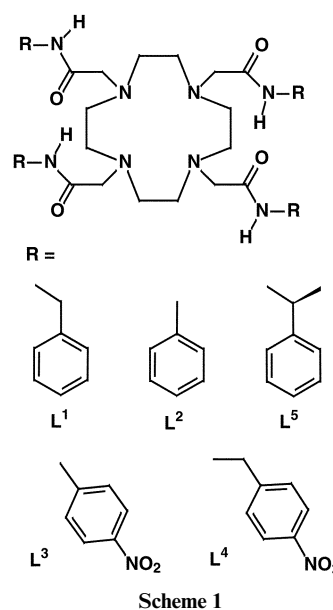
First published as an Advance Article on the web 18th June 2001

Comparative solid state structural studies of three lanthanide macrocyclic complexes derived from 1,4,7,10-tetraazacyclododecane with pendant arms bearing amide co-ordinating groups have been performed in order to evaluate the parameters influencing the co-ordination polyhedron and to assess the importance of the geometric factor in energy transfer processes. In all the investigated structures the co-ordination geometry is a mono-capped twisted square antiprism, a situation commonly observed for similar compounds. High resolution luminescence spectra of the europium complexes are consistent with a tetragonal site symmetry for the metal ion. An analysis of the presented crystal structures and of previously reported ones indicates that (i) the relative orientation of the O_4 and N_4 planes is not determined by the co-ordinated solvent molecule and (ii) the twist angle between them is mainly dictated by the flexibility of the pendant arms. Interpretation of the luminescence properties of the complexes of Sm(III), Eu(III) and Tb(III) can be made from the structural parameters found in the solid state and in solution (by NMR spectroscopy). Both the energy parameter (*i.e.* the gap between the ligand triplet state and the metal ion excited state) and the geometric parameter (*i.e.* the donor–acceptor distance and the orientation of the chromophore) have to be taken into account to explain the results obtained in terms of the efficiency of the $L \rightarrow Ln$ intra-molecular energy transfer. Furthermore, the correlative comparison between structural and luminescent properties shows how inter-molecular interactions in the solid state can be a prominent factor in the effectiveness of this transfer.

Introduction

Ligands based on the cyclen framework (cyclen is 1,4,7,10-tetraazacyclododecane) are ideal complexation agents for trivalent lanthanide ions. Besides stabilising the complexes by the macrocyclic effect, they fulfil the requirement of $Ln(III)$ for large co-ordination numbers.¹ The resulting edifices, strongly stable even in aqueous media,² are therefore particularly appropriate for analytical and/or medical uses, for instance as NMR shift reagents,³ magnetic resonance imaging contrast agents,^{4–6} radiolabels,⁷ or radiotracers.⁸ Some of the complexes, especially with the earlier lanthanides, have demonstrated a catalytic activity in the specific cleavage of RNA and DNA.^{9,10} Several luminescent lanthanide-containing chemosensors have recently been developed, based on cyclen complexes and in which modulation of the emission occurs *via* ligand- or metal-centred processes.¹¹ The design of such edifices requires a good command of the structural factors influencing their stability and photophysical properties and many structural studies have been reported on complexes with cyclen derivatives bearing pendant arms functionalized by carboxylate,^{12–15} phosphinate^{16–18} and amide^{19–24} co-ordinating groups. In these compounds the ion is the common vertex of two square pyramids, defined by O_4 , Ln and by N_4 , Ln and the resulting co-ordination geometry is a twisted square antiprismatic arrangement, often completed by a solvent molecule, which caps the plane defined by the oxygen atoms.

We are interested in designing stable luminescent complexes and in unravelling the relationship between structural and photophysical properties of lanthanide-containing edifices. Along these lines, we have recently described the properties of a tetra-amide ligand bearing benzyl moieties (L^1 , see Scheme 1)



† Electronic supplementary information (ESI) available: selected bond lengths and angles, intermolecular hydrogen bonds in $[Eu(L^2)(H_2O)]^{3+}$, excitation, emission and NMR spectra. See <http://www.rsc.org/suppdata/dt/b1/b101312m/>

and of its lanthanide complexes.²⁵ In this paper we pursue the analysis of similar systems by varying the length of the arms and/or the nature of the chromophoric groups in L^2 , L^3 and L^4

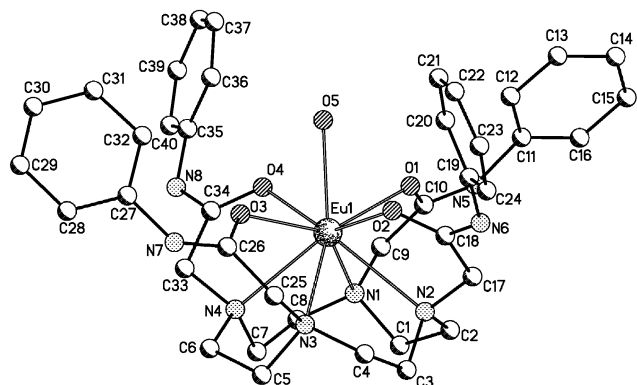


Fig. 1 Molecular structure and atom-numbering scheme for $[\text{Eu}(\text{L}^2)(\text{H}_2\text{O})]^{3+}$.

in order to determine the parameters influencing and controlling the photophysics of the complexes. We also hope to gain a better understanding of the energy migration processes occurring between the ligand and the lanthanide centre by comparing geometrical parameters with luminescence data.

Results and discussion

Ligands L^{2-4} have been obtained in 70–80% yield by treating the appropriate *N*-substituted bromoacetamide with cyclen in THF (L^2) or DMF ($\text{L}^{3,4}$) in the presence of an excess of triethylamine. The complexes were prepared in the usual way²⁵ by reaction of equimolar amounts of anhydrous lanthanide triflate (trifluoromethanesulfonate) and ligand. They were recrystallised from acetonitrile (L^2) or methanol ($\text{L}^{3,4}$) and gave satisfactory elemental analyses. Complexation of the four arms through the carbonyl functions is reflected by the $\nu(\text{C}=\text{O})$ vibration which is shifted towards lower energy by *ca.* 20 cm^{-1} upon complexation. Crystals suitable for structure determination could only be obtained with L^2 and L^3 .

Solid state structures

The complex $[\text{Eu}(\text{L}^2)(\text{H}_2\text{O})][\text{CF}_3\text{SO}_3]_3 \cdot 4\text{H}_2\text{O}$, EuL^2 , crystallises with four interstitial water molecules, two ordered triflate counter ions and two disordered half-triflates in the asymmetric unit. Ligand L^2 acts as an octadentate ligand and the metal ion completes its co-ordination sphere with one water molecule thus generating a nine-co-ordinate geometry. The atom numbering scheme is shown in Fig. 1. The Eu(III) is sandwiched between two almost parallel planes (interplanar angle = $0.4(1)^\circ$) defined by the four oxygen and the four nitrogen atoms. The average bond distance between the Eu(III) and the four amide oxygen atoms amounts to 2.379(5) Å, while the mean Ln–*N*(macrocycle) distance is longer, at 2.680(6) Å; the Ln–O(water) bond length is standard, at 2.431(5) Å, being very close to the one observed for similar tetra-amide cyclen derivatives.^{22,23,26} The europium ion lies closer to the plane defined by the oxygen atoms, as indicated by the distances to the mean O_4 and N_4 planes: 0.708(3) and 1.673(3) Å, respectively. This situation is partly due to the small cavity of the macrocycle and, possibly, to the harder nature of the O donor atoms. The distances between the *trans* nitrogen atoms, defining the size of the cavity, are 4.161(8) and 4.21(1) Å for $\text{N}1 \cdots \text{N}3$ and $\text{N}2 \cdots \text{N}4$, respectively. These values are too short for “in-plane” co-ordination of the europium ion.† The average values of the torsion angles NCCN in the macrocycle and NCCO in the pendant arms are $+59.4(9)$ and $-35.1(10)^\circ$, respectively, showing that the complex has crystallised in the $\Lambda(\delta\delta\delta\delta)$ form. The

† $4.18 \text{ \AA} < (2r(\text{Eu}^{3+}) + 2r(\text{N}))$, with $r(\text{Eu}^{3+}) = 1.12 \text{ \AA}$ for a co-ordination number of 9 and $r(\text{N}) = 1.32 \text{ \AA}$ for a co-ordination number of 4.

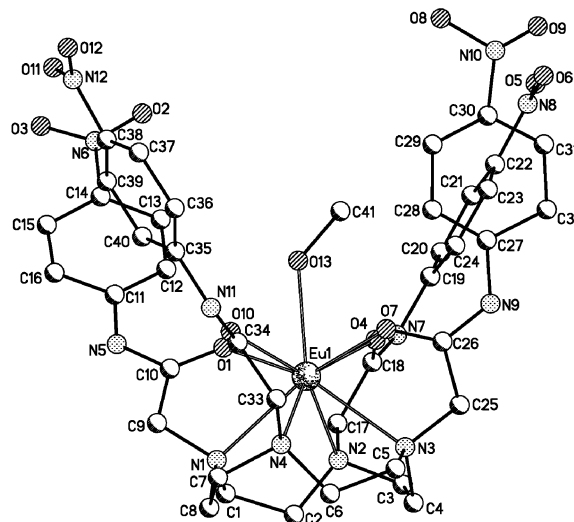


Fig. 2 Molecular structure and atom-numbering scheme for $[\text{Eu}(\text{L}^3)(\text{CH}_3\text{OH})]^{3+}$.

macrocycle adopts the stable [3333] conformation usually observed for twelve-membered rings with the nitrogen atoms at the corners.²⁷ The co-ordination polyhedron displays a twisted square antiprismatic arrangement of the four oxygen atoms and the four nitrogen atoms, with an average twist angle τ of 38.1° (compared to 0 and 45.0° for ideal square prismatic and antiprismatic arrangements, respectively). This leads to a distorted mono-capped antiprismatic geometry around the Eu(III). The amide hydrogen atoms are involved in hydrogen bonds with two triflate counter ions, one disordered half-triflate and one free water molecule. There is a network of hydrogen bonds connecting two neighbouring molecules *via* the co-ordinated water molecule (O5), the free water molecules Ow2, Ow3, Ow4 and the two ordered triflates (Table 1; Fig. S1, ESI). Thus, the crystal packing consists of a series of dimers.

The complex $[\text{Eu}(\text{L}^3)(\text{CH}_3\text{OH})][\text{CF}_3\text{SO}_3]_3 \cdot 2\text{CH}_3\text{OH}$, EuL^3 , crystallises with three triflate counter ions and two molecules of methanol. The crystals belong to the $P\bar{1}$ space group in the triclinic system, as do the europium,¹² gadolinium,²⁸ holmium,¹⁴ yttrium,²⁹ and lutetium^{30,31} complexes formed with DOTA (1,4,7,10-tetraazacyclododecanetetraacetate), a europium tetra(carboxyethyl) derivative of cyclen,¹³ and the dysprosium complex of DTMA (1,4,7,10-tetrakis(methylcarbamoylmethyl)-1,4,7,10-tetraazacyclododecane).²⁴ One methanol molecule is co-ordinated to the Eu(III) by capping the square plane of the co-ordinated oxygen atoms (Fig. 2). The metal ion is positioned 0.831(5) Å under the mean O_4 plane whereas it lies 1.624(6) Å above the N_4 plane. The two planes are almost parallel, the angle between them being $0.6(2)^\circ$. The average Eu–O and Eu–N distances are respectively 2.414(9) and 2.636(12) Å, while the Eu–O (CH_3OH) distance is 2.451(9) Å. The angle between the O_4 plane and the $\text{O}13\text{--Eu}1$ bond of the co-ordinated methanol molecule is 91.2° . The average values of the NCCN and NCCO torsion angles are both negative, $-56.9(15)^\circ$ and $-22.6(18)^\circ$, pointing to a $\Lambda(\lambda\lambda\lambda\lambda)$ conformation. The distances between the *trans* nitrogen atoms are 4.14(2) and 4.16(2) for $\text{N}1 \cdots \text{N}3$ and $\text{N}2 \cdots \text{N}4$, respectively, while the twist angle between the four oxygen and the four nitrogen atoms (25.5°) is indicative of a twisted square prismatic arrangement. As for EuL^2 , the crystal packing consists of dimers (Fig. 3) and is mainly determined by three types of hydrogen bonds (Table 1): (i) the first interaction occurs between interstitial methanol molecules and the NH groups of two amide functions, (ii) the two other amide H atoms interact with triflate counter ions, and (iii) two $[\text{Eu}(\text{L}^3)(\text{CH}_3\text{OH})]^{3+}$ molecules, related by an inversion centre, are linked by one nitro group of one cationic complex and interacting with a co-ordinated methanol molecule of the second one.

Table 1 Hydrogen bonds in the investigated crystal structures^a

D–H···A	<i>d</i> (D–H)/Å	<i>d</i> (H···A)/Å	<i>d</i> (D···A)/Å	<i>a</i> (DHA)/°
EuL²				
N5–H5···O12	0.88	2.12	2.89(2)	145.6
N6–H6···Ow1	0.88	2.26	3.01(1)	143.2
N7–H7···O6	0.88	2.11	2.922(9)	152.7
N8–H8···O9	0.88	2.26	2.825(9)	121.5
Ow1···O14#1			2.80(2)	
Ow1···O10#2			2.98(1)	
Ow1···Ow3#3			2.99(1)	
Ow2···Ow4#4			2.66(2)	
Ow2···O5			2.731(9)	
Ow2···Ow3#5			2.88(2)	
Ow2···O13#6			2.97(2)	
Ow3···O8			2.92(1)	
Ow4···O11			2.65(2)	
EuL³				
N(5)–H(5)···O(20)	0.88	1.96	2.825(17)	168.2
N(7)–H(7)···O(24)	0.88	1.96	2.774(18)	152.3
N(9)–H(9)···O(23)	0.88	1.87	2.74(2)	167.2
N(11)–H(11)···O(18)	0.88	1.93	2.786(17)	162.6
O(13)–H(13A)···O(3)#7	0.84	2.00	2.696(18)	139.0
O(23)–H(23A)···O(22)#8	0.84	2.01	2.792(19)	155.5
O(24)–H(24A)···O(15)#9	0.84	2.15	2.773(18)	131.3
LuL³				
N(5A)–H(5A)···O(13)#10	0.88	1.98	2.854(14)	176.2
N(7A)–H(7A)···O(28)#10	0.88	1.89	2.76(2)	176.5
N(9A)–H(9A)···O(19)#11	0.88	2.01	2.861(16)	162.2
N(11A)–H(11A)···O(34)	0.88	1.93	2.800(2)	168.4
O(13A)–H(13B)···O(3A)	0.84	2.40	2.885(16)	117.4
N(5B)–H(5B)···O(16)#12	0.88	1.98	2.854(14)	171.0
N(7B)–H(7B)···O(39)	0.88	1.92	2.80(2)	172.1
N(9B)–H(9B)···O(23)	0.88	2.05	2.92(2)	171.0
N(11B)–H(11B)···O(26)	0.88	1.83	2.70(2)	169.0

^a Symmetry operations: #1 $\frac{1}{2} - x, \frac{1}{2} - y, \frac{1}{2} - z$; #2 $x, \frac{1}{2} - y, \frac{1}{2} + y$; #3 $\frac{1}{2} - x, y, 1 - z$; #4 $-x, -y, -z$; #5 $x - \frac{1}{2}, -y, z$; #6 $\frac{1}{2} + x, -y, z$; #7 $-x, -y, -z + 1$; #8 $x - 1, y, z$; #9 $x, y - 1, z$; #10 $x + 1, y, z$; #11 $x - \frac{1}{2}, -y + \frac{1}{2}, z - \frac{1}{2}$; #12 $-x + \frac{1}{2}, y + \frac{1}{2}, -z + \frac{1}{2}$.

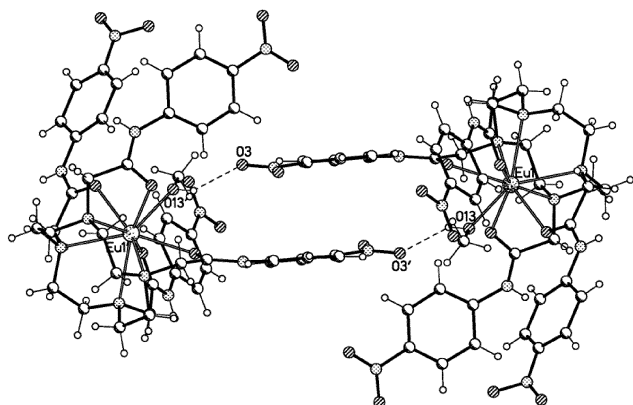


Fig. 3 Inter-molecular hydrogen bond occurring in $[\text{Eu}(\text{L}^3)(\text{CH}_3\text{OH})]^{3+}$ linking two neighbour molecules.

The asymmetric unit of $[\text{Lu}(\text{L}^3)(\text{CH}_3\text{OH})][\text{Lu}(\text{L}^3)(\text{H}_2\text{O})][\text{CF}_3\text{SO}_3]_6 \cdot 10\text{CH}_3\text{OH}$, **LuL³**, contains two different complexes, one with a methanol molecule co-ordinated ion (molecule A), while the other Lu(III) bears one water molecule (molecule B, Fig. 4). They are connected by only one hydrogen bond involving the co-ordinated water molecule and one oxygen atom of a nitro group. Therefore, as in the two complexes described above, the crystal packing consists of a series of dimers. The average Lu–O and Lu–N distances are 2.318(10) and 2.567(11) Å in A and 2.310(10) and 2.558(12) Å in B, respectively. The Lu–O (MeOH) distance is 2.347(9) Å, while the Lu–O (H₂O) is 2.368(10) Å. The absolute conformation of the two molecules is different: $\Lambda(\delta\delta\delta\delta)$ for A, with average NCCN and NCCO torsion angles of $+56.5(15)^\circ$ and $-26.7(14)^\circ$, and $\Delta(\lambda\lambda\lambda\lambda)$ for

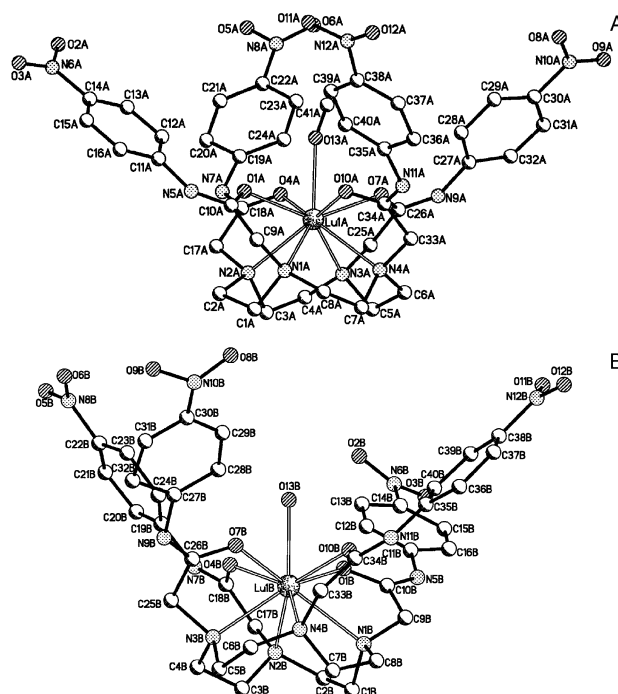


Fig. 4 Atom-numbering scheme for $[\text{Lu}(\text{L}^3)(\text{CH}_3\text{OH})]^{3+}$ (molecule A) and $[\text{Lu}(\text{L}^3)(\text{H}_2\text{O})]^{3+}$ (molecule B).

B, with average torsion angles of $-56.4(17)^\circ$ and $+28.1(16)^\circ$ for the NCCN and NCCO angles, respectively. The O atom of the water or methanol molecule lies on the C₄ axis going through Lu and Y, where Y is the centre of the O₄ plane. As in **EuL²** and

Table 2 Parameters characterising the square antiprismatic arrangements found in the investigated crystal structures (distances in Å and angles in °)^a

	[Eu(L ³)(H ₂ O)] ³⁺	[Eu(L ³)(CH ₃ OH)] ³⁺	[Lu(L ³)(CH ₃ OH)] ³⁺	[Lu(L ³)(H ₂ O)] ³⁺
<i>a</i>	90.0	90.0	90.0	90.0
<i>β</i>	103.9(3)	102.3(2)	107.8(2)	108.2(4)
<i>τ</i>	38.1	25.5	39.7	39.6
<i>δ</i>	51.9	64.5	50.3	50.4
<i>ε</i>	90.0	90.0	90.0	90.0
<i>φ</i>	177.9	179.0	177.7	177.9
<i>φ</i>	51.4	52.0	53.9	54.1
<i>π</i>	139.7(3)	145.4(2)	141.8(4)	140.0(4)
<i>θ</i>	72.7	69.9	70.9	70.0
<i>γ</i>	66.4(2)	63.0(3)	66.7(4)	67.0(4)
<i>Y</i> -O _{coord}	1.723	1.621	1.587(1)	1.576(1)
<i>a</i>	2.962(9)	2.93(2)	2.93(2)	2.93(2)
<i>b</i>	3.212(7)	3.21(1)	3.10(1)	3.07(2)
<i>c</i> (Ln1- <i>X</i>)	1.673(3)	1.624(6)	1.511(6)	1.499(6)
<i>d</i> (Ln1- <i>Y</i>)	0.708(3)	0.831(5)	0.759(5)	0.791(5)
N1...N3	4.161(8)	4.14(2)	4.118	4.142
N2...N4	4.21(1)	4.16(2)	4.182	4.145
Ln-O	2.379(5)	2.414(9)	2.318(10)	2.310(10)
Ln-N	2.680(6)	2.636(12)	2.567(11)	2.558(12)
Ln-O _{coord}	2.431(5)	2.451(9)	2.347(9)	2.368(10)

^a *X* and *Y* are respectively the centres of the N₄ and O₄ planes, O_{coord} is the supplementary co-ordinated molecule.

EuL³, the Lu(III) occupies the common vertex of two square pyramids and both co-ordination polyhedra can be described as distorted monocapped antiprisms, with very similar average twist angles of 39.7° (A), and 39.6° (B). For each sub-unit, four hydrogen bonds take place involving the amide hydrogen atoms (Table 1). No stacking interaction is evidenced between the two closest aromatic moieties of each sub-unit, the distance between the two centres being 4.79 Å and the angle between the two aromatic rings amounting to 23.5°.

Analysis of the co-ordination polyhedra

We have performed a quantitative analysis of the co-ordination polyhedra found in the investigated structures using the distances and angles presented in Fig. 5 and listed in Table 2 for each compound. In all cases, *X*, the centre of the N₄ plane, and *Y*, the centre of the O₄ plane, lie on the same line and define a C₄ axis which goes through the O atom of the solvent molecule co-ordinated in the ninth site (H₂O or MeOH). Ln-O distances are shorter than Ln-N distances with, as a consequence, *φ* being smaller than *θ*. Thus, the O₄Ln square pyramid is more flattened. The value of the angle *β* and the distances between the *trans* nitrogen atoms are too small to allow encapsulation of the Ln(III) in the cavity of the macrocycle; on the other hand, *π* is large enough to allow co-ordination of an additional small molecule. This angle is largest in **EuL³** to accommodate the bound methanol molecule.

Comparing [Eu(L³)(CH₃OH)]³⁺ with [Lu(L³)(CH₃OH)]³⁺ gives some insight into the influence of the ionic radius on the first co-ordination sphere. The obvious fact is the shorter Lu-O and Lu-N distances due to the smaller ionic radius of Lu(III). As a consequence, a tightening of the arms around the Lu(III) is observed and *β* becomes greater. However, the difference in the Ln-O distances is more pronounced than for the Ln-N distances because of the relative rigidity of the macrocycle and the ability of the flexible pendant arms to wrap more or less closely around the metal ion. Furthermore, we note that in both complexes the average Ln-O distances are smaller than the sum $r(\text{Ln}^{3+}) + r(\text{O}) = 2.36 \text{ \AA}$, and the Ln-N distances are larger than $r(\text{Ln}^{3+}) + r(\text{N}) = 2.44 \text{ \AA}$. This arises from the fact that the tertiary amine nitrogen atoms of the macrocycle are in a more rigid environment than the oxygen atoms which can rearrange and then adopt a favourable co-ordination geometry.³² Therefore, the *a* value is independent of the ionic radius of the metal ion. The comparison between [Lu(L³)(CH₃OH)]³⁺ and

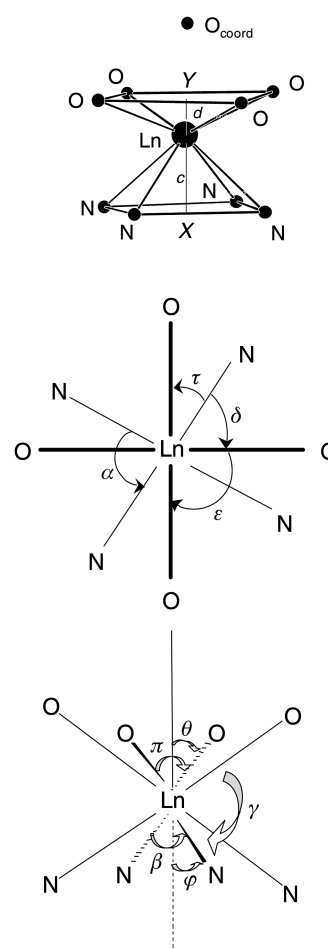


Fig. 5 Parameters defining a twisted square antiprismatic co-ordination polyhedron: relevant distances, spatial (↗) and projection (↘) angles; *X* and *Y* are the centres of the N₄ and O₄ planes, respectively.

[Lu(L³)(H₂O)]³⁺ does not show any drastic difference. Thus the relative orientation of the O₄ and N₄ planes is not governed by the supplementary co-ordinated molecule. The most remarkable difference found between the reported structures is the value of the angle *τ* which is 25.5° in [Eu(L³)(CH₃OH)]³⁺ whereas it varies between 38.1 and 39.7° in the other com-

Table 3 Absorption characteristics of compounds L²⁻⁴ and their complexes with Eu and Tb in dry and degassed acetonitrile at 293 K, and the energy of the singlet (S*) and triplet (T*) states at 77 K

Compound	$\pi \rightarrow \pi^*$ transitions, E^a/cm^{-1}	$E(\text{S}^*)/\text{cm}^{-1}$	$E(\text{T}^*)/\text{cm}^{-1}$
L ²	41 700 (4.72)	^c	22 800, ^b 24 400 ^c
L ³	44 840 (4.80), 40 650 sh (4.59), 33 300 (4.54)	35 000	26 100, ^b 19 800 ^b
L ⁴	47 100 (4.57), 36 500 (4.62)	35 250	22 350, ^b 24 100 ^d
EuL ²	41 500 (4.74)	34 600	25 700 ^b
TbL ²	41 150 (4.75)	34 600	^c
EuL ³	45 250 (4.75), 34 000 (4.80)	^c	^c
TbL ³	45 400 (4.65), 34 120 (4.71)	^c	^c
EuL ⁴	47 170 (4.56), 37 450 (4.58)	35 250	22 300 ^b
TbL ⁴	47 200 (4.45) 37 550 (4.48)		22 300 ^b

^a Maximum of band envelope; log ϵ is given within parentheses. The π - $\pi^*(\text{CO})$ band is seen between 50 000 and 54 000 cm^{-1} (log $\epsilon = 5.1$ – 5.3) for the “free” ligands. ^b Maximum of emission ^c Not observed. ^d 0-Phonon transition.

pounds. This is why the co-ordination polyhedron of $[\text{Eu}(\text{L}^3)(\text{CH}_3\text{OH})]^{3+}$ is closer to a twisted square prismatic arrangement.

Probing the local environment of the metal ion by high resolution luminescence

When dried under vacuum, the isolated complexes tend to lose their solvation molecule, as indicated by the vibrational spectra. This prompted us to use the europium(III) ion as a probe of its local environment by resorting to high resolution luminescence measurements on microcrystalline samples of dried **EuL²** and of undried **EuL³**. Non-selective excitation ($^5\text{L}_6 \leftarrow ^7\text{F}_{0,1}$ transitions, 10 K) of **EuL²** yields an emission spectrum similar to the one obtained for **EuL¹**.²⁵ The relative and corrected intensities of the $^5\text{D}_0 \rightarrow ^7\text{F}_J$ transitions ($J = 0$ – 4) are 0.21, 1.00, 1.33, 0.07, 1.52, respectively. The sizeable oscillator strength of the $^5\text{D}_0 \rightarrow ^7\text{F}_0$ transition is consistent with a C_n or C_{nv} point group of symmetry. The laser-excited excitation spectrum of the $^5\text{D}_0 \leftarrow ^7\text{F}_0$ transition displays one large band when monitored on the $^5\text{D}_0 \rightarrow ^7\text{F}_2$ transition (full width at half height, fwhh = 14 cm^{-1}), which is consistent with the presence of a single averaged environment for the Eu(III). Part of the broadening arises from vibronic components with energies similar to that of the $^7\text{F}_2$ state, as demonstrated by the excitation spectrum obtained upon monitoring the highest energy component of the $^5\text{D}_0 \rightarrow ^7\text{F}_1$ transition. In this case the excitation band is narrower: fwhh = 9 cm^{-1} . The energy of the $^5\text{D}_0 \leftarrow ^7\text{F}_0$ transition recorded at room temperature ($\tilde{\nu} = 17\,244 \text{ cm}^{-1}$) allows us to assess the co-ordination number of the Eu(III) on the basis of the nephelauxetic effect: $\tilde{\nu} - \tilde{\nu}_0 = C_{\text{CN}} \sum n_i \rho_i$; $C_{\text{CN}} = 1.06$ for a co-ordination number of 8, n_i is the number of donor atoms of type i , the ρ_i parameters represent the nephelauxetic effect induced by each donor atom, and $\tilde{\nu}_0$ is equal to 17 374 cm^{-1} .³³ The calculated position of the $^5\text{D}_0$ level for a co-ordination number (CN) of eight, using $\delta_{\text{C-O}} = -16.6 \text{ cm}^{-1}$ and $\delta_{\text{N}} = -12.8 \text{ cm}^{-1}$,³³ is 17 249 cm^{-1} , in good agreement with the experimental one, showing that there is no bound water molecule in the solid state after drying the compound and consistent with the decay rate constants of the $^5\text{D}_0$ excited state obtained for dried and undried crystals (see below). Recalculating the nephelauxetic parameter from our data, we find $\delta_{\text{N-cyclen}} = -14.1 \text{ cm}^{-1}$, a value close to those reported for other complexes with cyclen derivatives (-13.6 to -14.3 cm^{-1}).³⁴

The emission spectrum of **EuL³** displays much sharper bands than those of **EuL¹** and **EuL²**, but the relative intensities of the $^5\text{D}_0 \rightarrow ^7\text{F}_J$ transitions ($J = 0$ – 4) are similar: 0.19, 1.00, 1.46, 0.07, 1.75, respectively at 10 K (Fig. S2, ESI). The $^5\text{D}_0 \leftarrow ^7\text{F}_0$ excitation spectrum presents a very narrow symmetrical band (fwhh = 1 cm^{-1}) pointing to a single well defined europium(III) site. Under selective laser excitation, the $^5\text{D}_0 \rightarrow ^7\text{F}_1$ transition displays two components while the $^5\text{D}_0 \rightarrow ^7\text{F}_4$ transition presents four components assigned to two E-type (each displaying a narrow splitting) and two A-type, consistent with a

pseudo C_{4v} symmetry. At room temperature, the energy of the $^5\text{D}_0 \leftarrow ^7\text{F}_0$ transition amounts to 17 233 cm^{-1} (fwhh = 4 cm^{-1}), closer to the calculated value of 17 228 cm^{-1} for a CN of nine ($\delta_{\text{N}} = -17.8 \text{ cm}^{-1}$),³⁴ taking into account the bound methanol molecule, than to the calculated value of 17 244 cm^{-1} for CN = 8, without a co-ordinated methanol molecule.

Photophysical properties of ligands L²⁻⁴ and of the complexes with L²⁻³ in the solid state

The absorption spectral data in acetonitrile are reported in Table 3. They indicate that complexation induces minor shifts in the energy of the transitions and small variation in their intensity. We note that molar absorption coefficients of the lanthanide complexes are large, a favourable condition for an efficient antenna effect.

At room temperature, no emission from the “free” ligands is seen, neither in the solid state nor in solution. On the other hand, the ligands display a weak luminescence at 77 K (Fig. S3, ESI). The maximum of the singlet state emission occurs at 35 000 cm^{-1} for L³ and 35 250 cm^{-1} for L⁴, but no fluorescence band appears in the emission spectrum of L². The maximum of the triplet state emission is found at 24 400 cm^{-1} for L² and 24 100 cm^{-1} for L⁴, while two emission bands are observed for L³, the most intense having a maximum at 26 100 cm^{-1} , while the second one appears at 19 800 cm^{-1} with a very weak intensity. The excitation spectrum recorded upon monitoring the latter displays a maximum at 27 800 cm^{-1} which is also seen for the complexes (see below). We think that the triplet state with the highest energy is due to electronic density mainly localised on the aromatic rings, as for L² and L⁴, while the lowest energy one may be explained by the presence of a molecular orbital involving the nitro groups. We have no explanation why such a triplet state is not seen for L⁴. The energies of the observed excited states of the “free” and complexed ligand are reported in Table 3.

When Lⁱ are complexed to luminescent Ln(III) the ligand luminescence is strongly affected by the energy transfer to the metal ion. **LnL²** complexes have a similar luminescence behaviour to that previously described for complexes formed with L¹. In both series of complexes the ligand fluorescence remains relatively important, pointing to a not so efficient inter-system crossing. The first excited singlet state is found at 34 600 cm^{-1} (maximum of the emission band). Furthermore, emission from the triplet state (25 700 cm^{-1}) is also important in the europium(III) complex, partly because of a poor triplet-to-Eu(III) energy transfer (Fig. 6).

Excitation spectra of the **LnL³** complexes in the solid state (Ln = Sm, Eu or Tb) display only one broad ligand-centred band with a maximum at 27 850 cm^{-1} , indicating that the L \rightarrow Ln energy transfer goes through the triplet state involving the nitro groups (Fig. 7). The Eu(III) emits relatively strongly in the solid state at room temperature, which is not the case of Tb(III), pointing to a main energy transfer path going

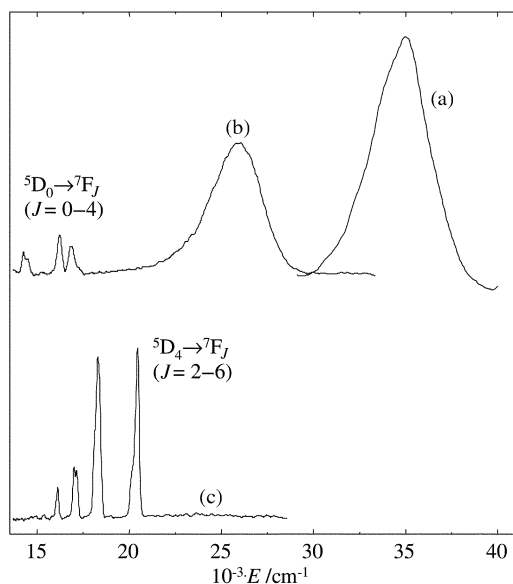


Fig. 6 Fluorescence (a) and phosphorescence (b) spectra of EuL^2 , and phosphorescence (c) spectrum of TbL^2 (solid state, 77 K). The following excitation energies, time delays and bandpaths were used: (a) 42 373 cm^{-1} , 0 μs , 4 nm; (b) 42 553 cm^{-1} , 20 μs , 10 nm; (c) 35 714 cm^{-1} , 20 μs , 2.5 nm.

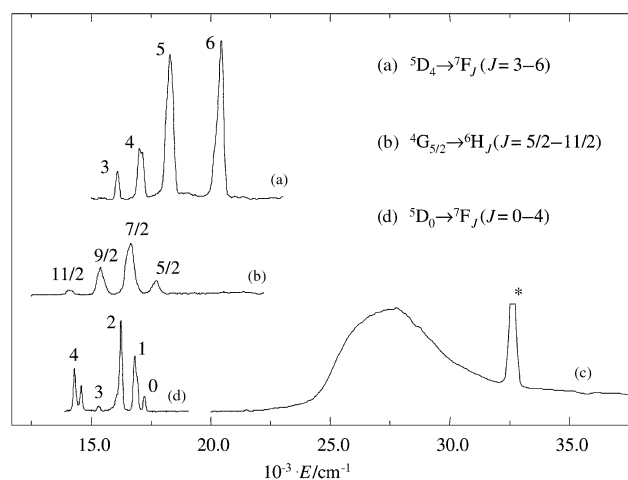


Fig. 7 Emission spectra of TbL^3 (a), SmL^3 (b) and EuL^3 (d) in the solid state at 77 K, and excitation spectrum of EuL^3 (c, $E_{\text{an}} = 16\,234\text{ cm}^{-1}$). The following excitation energies, time delays and bandpaths were used: 29 155 cm^{-1} , 60 μs , 10 nm (a), 28 165 cm^{-1} , 10 μs , 5 nm (b), 25 316 cm^{-1} , 60 μs , 5 nm, 1% attenuator (d). The asterisk refers to the Rayleigh diffusion band.

through this low-lying $^3\text{T}^*(\text{NO}_2)$ state. The energy gap $^5\text{D}_4(\text{Tb}) - ^3\text{T}^*(\text{NO}_2)$ could not be estimated because no emission from the lowest triplet state is observed in the complexes, even with non-luminescent ions. A proof of this proposed sensitisation mechanism is further given by the fact that terbium(III) emission is decreasing exponentially with increasing temperature, a phenomenon characteristic of a thermally activated $^5\text{D}_4(\text{Tb})$ -to- $^3\text{T}^*(\text{NO}_2)$ back transfer. The activation energy of the latter process, as determined by measuring the $^5\text{D}_4$ de-activation rate *versus* temperature, amounts to $1076 \pm 37\text{ cm}^{-1}$ for a solid state sample, a value that should approximately match the $^5\text{D}_4(\text{Tb}) - ^3\text{T}^*(\text{NO}_2)$ energy difference (Fig. S4, ESI). The relatively intense emission of Eu(III) in the solid state can be partially explained by the proximity of $^3\text{T}^*(\text{NO}_2)$ with $^5\text{D}_0(\text{Eu})$, the energy gap being smaller than in $\text{EuL}^{1,2}$. We have also studied the samarium(III) complex because its $^4\text{G}_{5/2}$ acceptor level lies around 550 cm^{-1} higher in energy than the $^5\text{D}_0(\text{Eu})$ level, so a sizeable $\text{L} \rightarrow \text{Sm}$ energy transfer was expected. Its emission spectrum displays the characteristic $^4\text{G}_{5/2} \rightarrow ^6\text{H}_j$

transitions ($J = \frac{5}{2} - \frac{11}{2}$, Fig. 7), and no luminescence from the ligand is observed.

To assess the importance of the non-radiative de-excitation processes, we have measured the decay rate constants of solid state samples of the complexes with Sm, Eu and Tb (Table 4). All the luminescence decays could be fitted satisfactorily with single exponential decay laws. As expected from the small energy gap between $^4\text{G}_{5/2}$ and $^6\text{F}_{11/2}$ (*ca.* 7 200 cm^{-1}), the de-activation rate constant of SmL^3 is large, lifetimes of the excited state level being in the range 22–27 μs only. De-activation rate constants for the dried sample of EuL^2 are small, only slightly temperature-dependent and comparable to those found for EuL^1 ,²⁵ reflecting that no water is co-ordinated to the metal ion, while the rate constant for the undried sample is substantially larger. In the case of the dried sample of EuL^3 the decay constants are about double those for dried EuL^2 , and they are even larger than for undried EuL^2 , reflecting the presence of additional de-activation paths. Back transfer to the ligand triplet state does not seem to play a large role since the rate constants are not very temperature dependent, but photo-induced electron transfer (PET) processes could be operative with this ion. In particular, we suspect such a process involving the ligand singlet state and the Eu(III) because of the higher absorption coefficients found in the absorption spectrum of EuL^3 , which could be indicative of the presence of a charge transfer. The de-activation rate constant for TbL^2 lies indeed in the expected range for this type of compound (*cf.* 0.53 ms^{-1} for $\text{TbL}^{1,25}$). In the case of TbL^3 , the larger decay constant can be explained by an efficient back transfer process (see above), while the rate constant measured for TbL^4 is closer to that observed for the compounds with $\text{L}^{1,2}$. Generally speaking, the rate constants for the terbium(III) edifices are smaller than those for the europium(III) complexes in view of the larger energy gap between the lowest sub-level of the excited state and the highest sub-level of the ground state in the former ion.

Structural properties of the complexes in solution

In order to rationalise the photophysical behaviour of the complexes in solution, we have first attempted to establish their structure in solution. We have taken the complexes of Eu(III) and Lu(III) as models since their NMR spectra can easily be assigned and since we have solid state structures for the complexes with L^2 and L^3 . The NMR spectra of the complexes are consistent with an average C_4 -symmetry at 293 K (see Experimental section) which leads us to conclude that the complexes adopt in solution a conformation similar to the one found in the crystal structures. However, upon lowering the temperature, spectra are obtained for Eu(III) which are characteristic of an equilibrium between isomers, a commonly observed fact for such systems.^{35,36} In the spectra of the lutetium(III) complexes the methylenic protons display broad signals at room temperature, pointing to this ion being in a somewhat more labile environment but only one isomer is present, even at low temperature (ESI, Fig. S5).

To render the comparison between solid state and solution structure more quantitative, we have evaluated the distance r between the aromatic protons and Eu(III) in EuL^2 in D_2O by determining the longitudinal relaxation times T_1 and using the equation:³⁷ $(1/T_1)_p - (1/T_1)_d = k/r^6$ where the indices p and d stand for paramagnetic and diamagnetic complexes, respectively. The values obtained for the europium(III) complex amount to 1.321, 1.139 and 0.182 s for the *para*, *meta* and *ortho* protons, respectively. The corresponding values could not be determined for the lutetium(III) complex because the signals are not separated. Therefore we have chosen the proton in the *para* position as a reference because it is less influenced by the paramagnetism of the Eu(III), which allowed us to estimate k and the distances between Eu(III) and the *ortho* and *meta* protons: 5.87 and 7.97 Å, respectively. The respective average

Table 4 Observed decay rate constants of the $\text{Eu}({}^5\text{D}_0)$, $\text{Tb}({}^5\text{D}_4)$ and $\text{Sm}({}^4\text{G}_{5/2})$ excited levels in $\text{Ln}(\text{L}^{2,3,4})$ ($\text{Ln} = \text{Eu}, \text{Tb}$ or Sm) under various experimental conditions

LnL^i	Conditions	T/K	$E_{\text{exc}}/\text{cm}^{-1}$	k/ms^{-1}
EuL²	Dried crystals	77	17 258	0.89 ± 0.02
	Dried crystals	293	17 258	0.96 ± 0.02
	Dried crystals	77	42 553	0.94 ± 0.07
	Dried crystals	293	42 553	1.09 ± 0.07
	Undried crystals	293	42 553	1.67 ± 0.11
	$1.1 \times 10^{-3} \text{ M}/\text{CH}_3\text{CN}^a$	293	42 373	1.05 ± 0.04
TbL²	Dried crystals	293	35 714	0.54 ± 0.01
	Dried crystals	77	37 037	0.55 ± 0.07
	$1.1 \times 10^{-3} \text{ M}/\text{CH}_3\text{CN}^a$	293	34 483	0.42 ± 0.01
	$1.3 \times 10^{-3} \text{ M}/\text{Water}$	293	34 483	0.62 ± 0.02
	$1.2 \times 10^{-3} \text{ M}/\text{D}_2\text{O}$	293	34 247	0.37 ± 0.02
EuL³	Dried crystals	77	17 238	1.92 ± 0.07
	Dried crystals	77	25 974	2.04 ± 0.07
	Dried crystals	293	25 707	2.22 ± 0.10
	$1.0 \times 10^{-3} \text{ M}/\text{CH}_3\text{CN}^a$	293	26 667	1.12 ± 0.05
	$8.6 \times 10^{-4} \text{ M}/\text{D}_2\text{O}$	293	26 667	1.30 ± 0.03
	$1.0 \times 10^{-3} \text{ M}/\text{Water}$	293	26 667	2.27 ± 0.10
TbL³	Dried crystals	77	28 011	0.87 ± 0.03
	Dried crystals	293	28 011	20.8 ± 1.7
SmL³	Dried crystals	77	28 169	45.2 ± 4.1
SmL³	Dried crystals	293	28 011	37.5 ± 0.3
EuL⁴	$5 \times 10^{-5} \text{ M}/\text{CH}_3\text{CN}^a$	77	41 667	1.12 ± 0.05
TbL⁴	$5 \times 10^{-5} \text{ M}/\text{CH}_3\text{CN}^a$	77	41 667	0.72 ± 0.04
TbL⁴	Dried crystals	30–290	20 530	0.71 ± 0.02

^a Dried and degassed CH_3CN (≈ 15 ppm of water).

Table 5 Quantum yields measured for LnL^i , $\text{Ln} = \text{Eu}$ or Tb ; $i = 1-4$, in dry and degassed acetonitrile at 293 K

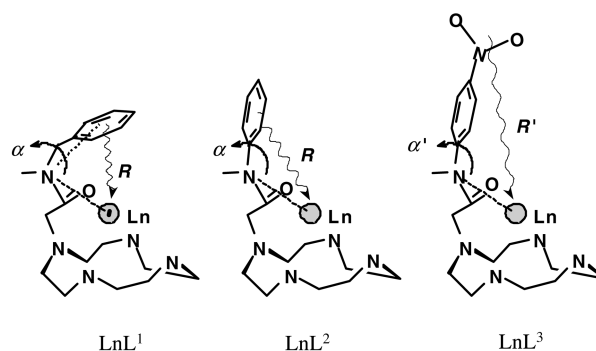
LnL^i	Φ_{abs} (%)	LnL^i	Φ_{abs} (%)
EuL¹	0.06 ^a	TbL¹	6.4 ^a
EuL²	0.02	TbL²	0.22
EuL³	0.003	TbL³	5×10^{-3}
EuL⁴	^b	TbL⁴	5.6×10^{-2}

^a Ref. 25. ^b Too low to be measured.

values obtained by X-ray diffraction are 5.63 and 7.43 Å. We therefore conclude that the average structure in solution is close to the one observed in the solid state and that this is most probably true for all the complexes we are investigating.

Photophysical properties of the complexes in solution

The absolute quantum yields of the complexes in water are listed in Table 5. All the europium(III) complexes are poorly luminescent, which can be traced back, at least in part, to the relatively high energy of the triplet state in the complexes with $\text{L}^{1,2,4}$. The values found for LnL^1 and LnL^2 may be rationalised as follows. The efficiency of the $\text{L} \rightarrow \text{Ln}$ energy transfer depends on energetic and geometric factors. In fact, the former are not very different in the two complexes, $\Delta E({}^3\pi\pi^* \rightarrow {}^5\text{D}_0)$ being equal to 9 000 and 8 750 cm^{-1} in **EuL¹**²⁵ and **EuL²**, respectively. Therefore the 2.5 fold larger quantum yield exhibited by **EuL¹** must arise from a better positioning of the chromophoric groups. Comparing the crystal structures of **EuL⁵** (taken as model for **EuL¹**)²² and **EuL²** we indeed evidence the importance of the spacer methylenic group between the amide function and the aromatic moiety. It allows the arms to bend and the chromophoric groups adopt a much better conformation for an efficient through space transfer onto the metal ion (Fig. 8). We have defined R as the average distance between the centre of the aromatic ring and the lanthanide(III) ion while the average angle between the metal ion, the amide nitrogen atom and the centre of the aromatic moiety and the nitro group has been labelled α and α' , respectively. These parameters amount to $R = 5.93$ and 6.23 Å and $\alpha = 92.0$ and 115.2° for **EuL⁵** and **EuL²**, respectively. Assuming that the energy transfer is operative *via* a through

**Fig. 8** Schematic representation of the $\text{L}^i \rightarrow \text{Ln}$ energy transfer in LnL^i complexes (left, $i = 1$; centre, $i = 2$; right, $i = 3$).

space dipole–dipole (Förster) mechanism,³⁸ the improvement expected on the sole basis of the shorter R distance in **EuL¹** is calculated to be 1.3. The remaining factor (1.9) is therefore attributable to the better orientation of the chromophore in **EuL¹**, which is almost perpendicular to the C_4 axis of the molecule.

EuL³ exhibits surprising luminescence properties. Its quantum yield is very low, but it displays a strong europium(III) solid state luminescence intensity upon ligand excitation. The former can be explained by the long distance R' between the centre of the NO_2 group (where the orbital describing the low-lying triplet state is mostly located) and the metal ion (9.82 Å): a calculation similar to the one above predicts a quantum yield 15 times smaller than for **EuL²** (α' is similar to the corresponding α angle in **EuL²**, 117.2°) an unfavourable factor which more than overcomes the energetic factor, expressed by a smaller, favourable, energy gap $\Delta E({}^3\text{T}^* \rightarrow {}^5\text{D}_0)$ estimated to 2 500 cm^{-1} (from the maximum of the ${}^3\text{T}^*$ emission in the “free” ligand data). On the other hand, we think that the relatively strong luminescence emitted in the solid state (and visible to the naked eye) can be explained by an inter-molecular energy transfer from the ${}^3\text{T}^*(\text{NO}_2)$ state of one molecule to the europium centre of a neighbouring one, the distance between the sensitiser and the metallic acceptor (4.79 Å) being much shorter than the intramolecular one. This process is favoured by the presence of a hydrogen bond between one nitro group and the co-ordinated

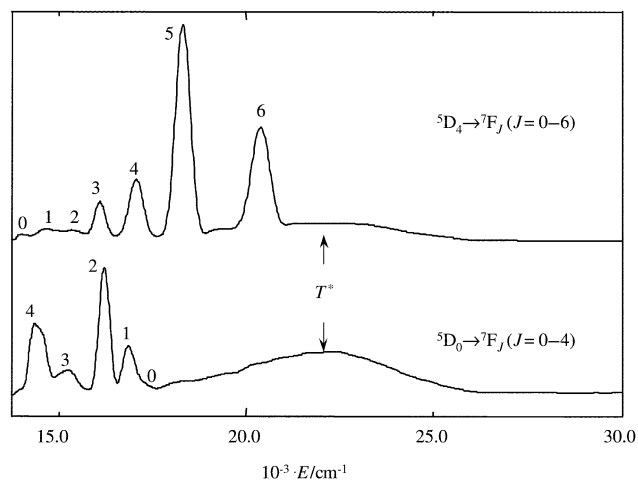


Fig. 9 Phosphorescence spectra of TbL^4 (top) and EuL^4 (bottom), 5×10^{-5} M in CH_3CN at 77 K, $E_{\text{exc}} = 41\,667\text{ cm}^{-1}$, time delay = 50 μs , bandpath = 5 nm.

methanol molecule of a neighbouring complex (Fig. 3). Ligand L^4 and its complexes have been synthesized to support this explanation, with respect to the properties of LnL^3 . It turned out that the europium(III) complex exhibits an extremely poor luminescence, both in the solid state and in solution. This is explained by the existence of only one triplet state occurring at $22\,300\text{ cm}^{-1}$ for the complexes (maximum of the emission band, Fig. 9). The resulting $\Delta E(^3\pi\pi^* - ^5\text{D}_0)$ gap of $5\,070\text{ cm}^{-1}$ (a value which is in reality larger if we take into account the 0-phonon transition) is usually not considered to be extremely favourable to an efficient energy transfer from the ligand to Eu(III); emission from the triplet state is seen in the luminescence spectrum, the ratio between the intensity of the metal-centered luminescence and that from the triplet state being around 0.7 : 1.

The situation for the terbium(III) complexes is similar to that discussed for Eu(III) as far as the complexes with L^1 and L^2 are concerned: both the energy factor ($\Delta E(^3\pi\pi^* - ^5\text{D}_4) = 5600$ and 5500 cm^{-1} , respectively, considering the maxima of triplet state emission) and the geometric factor are more favourable for L^1 , which explains the 30-fold smaller quantum yield for TbL^2 . The 40-fold decrease in quantum yield upon going from TbL^2 to TbL^3 is easily explained by the back transfer process quantified in the solid state (see above) while the tenfold larger quantum yield of TbL^4 with respect to TbL^3 may be explained both by a better orientation of the chromophoric group and a better energy factor. Finally, the measured radiative rates in water and D_2O for the TbL^2 and EuL^3 complexes are consistent with one co-ordinated water molecule: applying the proposed formula for this type of compounds,³⁹ we find hydration numbers $q = 0.95$ and 0.86 , respectively.

Conclusion

In all the complexes discussed here the macrocyclic nitrogen atoms and the amide oxygen atoms define two squares, the latter being capped by a solvent molecule, leading to a co-ordination number of nine. Thus, all the compounds adopt a twisted square antiprismatic arrangement around the metallic centre. This co-ordination is imposed by the design of the ligand and its co-ordinating atoms. For instance, when the amide function is replaced by phosphinate, the latter creates a steric hindrance which prevents co-ordination of an additional molecule with the same Ln(III).¹⁷ Comparing the solid state structures of two complexes with the same ligand but two different ions, $[\text{Eu}(\text{L}^3)(\text{CH}_3\text{OH})]^{3+}$ and $[\text{Lu}(\text{L}^3)(\text{CH}_3\text{OH})]^{3+}$, we do not observe any important changes in the first co-ordination sphere, except for smaller distances between the Lu(III) and the co-ordinating atoms. High-resolution luminescence measure-

ments confirm the tetragonal site symmetry of the europium(III) ion evidenced by crystallographic data. Our photophysical investigations show that both energy and geometric parameters must be taken in consideration to describe precisely the $\text{L} \rightarrow \text{Ln}$ energy transfer efficiency. The latter can be very different for the same compound, depending on the solvation, as shown for EuL^3 . We conclude that both sets of parameters must be well characterised to explain and understand the photophysical properties of the complexes with ligands derived from cyclen. In addition, a sensitive design of a lanthanide-containing luminescent probe will also have to take into account the efficiency of the inter-system crossing from singlet to triplet states, a matter that is not documented here, but that we have discussed recently.⁴⁰

Experimental

Synthesis and characterisations

Solvents and chemicals were purchased from Fluka AG (Buchs, Switzerland). Acetonitrile was treated by CaH_2 and P_2O_5 .⁴¹ Dichloromethane and tetrahydrofuran were distilled from CaH_2 . Lanthanide trifluoromethanesulfonates (triflates) were prepared from the oxides (Rhône-Poulenc, 99.99%) and triflic acid.⁴² Elemental analyses were performed by Dr H. Eder of the Microchemical Laboratory of the University of Geneva.

1,4,7,10-Tetraazacyclododecane⁴³ and L^1 were synthesized as previously described.²⁵

N-(Phenyl)bromoacetamide was prepared in 92% yield using the method of Hamada *et al.*⁴⁴ with bromoacetyl bromide instead of chloroacetyl chloride. TLC: 1 spot, $R_f = 0.76$ (5% MeOH in CH_2Cl_2). δ_{H} (CDCl_3) 4.01 (s, 2H, BrCH_2), 7.16 (t, $^2J = 7.5$, 1H, Ar), 7.35 (t, $^2J = 7.5$, 2H, Ar), 7.52 (d, $^2J = 7.5$ Hz, 2H, Ar). Mp $133.5\text{--}134.5\text{ }^\circ\text{C}$.

1,4,7,10-Tetrakis[*N*-(phenyl)carbamoylmethyl]-1,4,7,10-tetraazacyclododecane (L^2). A mixture of 1 equivalent of cyclen (0.517 g, 3.0 mmol), 4 equivalents of *N*-(phenyl)bromoacetamide (2.569 g, 12.0 mmol) and 5 equivalents of triethylamine (2.091 cm^3 , 15.0 mmol) in 50 cm^3 of dry tetrahydrofuran was refluxed for 20 h under nitrogen. After evaporation of the solvent, the residue was partitioned between 100 cm^3 of water and 100 cm^3 of CH_2Cl_2 . The organic phase was evaporated and the remaining solid dissolved in 6 cm^3 of hot dimethylformamide; 20 cm^3 of water were added and the cloudy solution was heated until boiling. Upon cooling, a white solid precipitated and was filtered off. After drying (8 h, 1 mbar, 333 K), 1.640 g of L^2 were collected (yield 78%). Found: C, 68.07; H, 6.92; N, 15.65. Calc. for $\text{C}_{40}\text{H}_{48}\text{N}_8\text{O}_4$: C, 68.15; H, 6.87; N, 15.90%; δ_{H} (CD_3CN , 295 K) 2.90 (s, 4H, NCH_2), 3.23 (s, 2H, NCH_2CO), 7.01 (t, 1H, Ar), 7.19 (t, $^2J = 7.5$, 2H, Ar), 7.49 (d, $^2J = 8.5$ Hz, 2H, Ar), 9.20 (s, 1H, NH). mp $201\text{--}203\text{ }^\circ\text{C}$. ν_{max} 3290 (NH), 1634 cm^{-1} (C=O).

***N*-(4-Nitrophenyl)bromoacetamide.** A mixture of *p*-nitroaniline (5.525 g, 40.0 mmol) and dry pyridine (4.0 cm^3 , 50.0 mmol) in 250 cm^3 of dry tetrahydrofuran was ice-cooled. A solution of bromoacetyl bromide (8.074 g, 40.0 mmol) in 15 cm^3 of dry tetrahydrofuran was slowly added and the resulting mixture stirred for 1 h at 273 K, then 1 h at 298 K. The solution was filtered and concentrated to 50 cm^3 . Then 50 cm^3 of water were added and the solution was allowed to stand overnight at 274 K. The orange-yellow solid was filtered and recrystallised in 100 cm^3 of acetone-water (2 : 3, v/v). After drying (8 h, 1 mbar, 328 K), 7.190 g were obtained (yield: 69%). $R_f = 0.20$ (CH_2Cl_2). δ_{H} ($\text{DMSO}-d_6$, 295 K) 4.11 (s, 2H, BrCH_2), 7.83 (d, $^2J = 9.0$, 2H, Ar), 8.24 (d, $^2J = 9.0$ Hz, 2H, Ar), 11.00 (s, 1H, NH). mp $174.0\text{--}175.5\text{ }^\circ\text{C}$.

1,4,7,10-Tetrakis[*N*-(4-nitrophenyl)carbamoylmethyl]-1,4,7,10-tetraazacyclododecane (L^3). A mixture of 1 equivalent of

cyclen (0.517 g, 3.0 mmol), 4 equivalents of *N*-(4-nitrophenyl)-bromoacetamide (3.109 g, 12.0 mmol) and 8 equivalents of triethylamine (3.345 cm³, 24.0 mmol) in 150 cm³ of DMF was heated for 14 h at 358 K. 500 cm³ of water were added and the solution was heated at 373 K during 0.5 h. After cooling, the beige precipitate was filtered, washed with 20 cm³ of H₂O and dried (8 h, 1 mbar, 298 K). The solid was suspended in 35 cm³ of DMF and 25 cm³ of water and the mixture heated at 373 K during 0.5 h. After cooling, the solid was filtered off and dried (8 h, 1 mbar, 298 K) to give 1.830 g of L³ (yield 69%). Found: C, 54.02; H, 5.28; N, 18.68. Calc. for C₄₀H₄₄N₁₂O₁₂: C, 54.30; H, 5.01; N, 19.00%; δ_H (DMSO-*d*₆, 295 K) 3.33 (s, 4H, NCH₂), 3.36 (s, 2H, NCH₂CO), 7.76 (d, ²*J* = 9.1, 2H, Ar), 8.11 (d, ²*J* = 9.1 Hz, 2H, Ar), 10.50 (s, 1H, NH). mp > 230 °C. ν_{max} 3284 (NH), 1651 (C=O), 1523 and 1351 cm⁻¹ (NO₂).

***N*-(4-Nitrobenzyl)bromoacetamide.** A mixture of 0.419 g (10.5 mmol) of NaOH in 10 cm³ of water and 1.000 g (5.3 mmol) of 4-nitrobenzylamine hydrochloride in 100 cm³ of CH₂Cl₂ was ice-cooled. A solution of bromoacetyl bromide (1.070 g, 5.3 mmol) in 10 cm³ of CH₂Cl₂ was slowly added and the resulting mixture stirred for 1 h at 273 K, then 1 h at 298 K. The organic phase was washed twice with 100 cm³ of water, dried over Na₂SO₄ and evaporated. The white solid was recrystallised in 30 cm³ of acetone–water (2 : 3, v/v). After drying (8 h, 1 mbar, 328 K), 1.170 g were obtained (yield: 81%). Found: C, 39.71; H, 3.56; N, 10.10. Calc. for C₉H₉BrN₂O₃: C, 39.58; H, 3.32; N, 10.26%. δ_H (CDCl₃, 295 K) 3.97 (s, 2H, BrCH₂), 4.59 (d, 2H, ²*J* = 6.4, NCH₂Ar), 6.92 (s, br, 1H, NH), 7.46 (d, 2H, ²*J* = 8.6, Ar), 8.21 (d, 2H, ²*J* = 8.6 Hz, Ar).

1,4,7,10-Tetrakis[*N*-(4-nitrobenzyl)carbamoylmethyl]-1,4,7,10-tetraazacyclododecane (L⁴). This was synthesized in 70% yield using the same procedure as described for L³ and recrystallised in dichloromethane–ethanol (1 : 1, v/v). Found: C, 55.82; H, 5.39; N, 18.02. C₄₄H₅₂N₁₂O₁₂ requires: C, 56.16; H, 5.57; N, 17.86%. δ_H (DMSO-*d*₆, 295 K) 2.62 (s, 4H, NCH₂), 3.04 (s, 2H, NCH₂CO), 4.33 (d, 2H, NCH₂Ar), 7.41 (d, ²*J* = 8.4, 2H, Ar), 8.11 (d, ²*J* = 8.4 Hz, 2H, Ar), 8.58 (t, 1H, NH). ν_{max} = 3270 (NH), 1650 (C=O), 1520 and 1345 cm⁻¹ (NO₂).

Complexes. [Ln(L^{*i*})](CF₃SO₃)₃ (*i* = 2, 3 or 4) were prepared by heating under reflux 1 equivalent of the lanthanide salt and 1 equivalent of L^{*i*} in dry acetonitrile. After cooling, the solution was filtered and concentrated, dichloromethane was added and the resulting solution kept overnight at 277 K. The deposited solid was recovered by filtration, washed with dichloromethane and dried (2 h, 1 mbar, 313 K). Complexes with L² were re-crystallised from acetonitrile and with L^{3,4} from methanol (yields 60–65%).

[Eu(L²)](CF₃SO₃)₃. Found: C, 39.49; H, 4.00; N, 8.38. Calc. for C₄₃H₄₈EuF₉N₈O₁₃S₃: C, 39.57; H, 3.71; N, 8.59%. δ_H (CD₃CN, 293 K) 20.58 (s, br, 1H, ax. ring CH₂), 7.86 (s, 2H, Ar), 7.52 (s, 1H, Ar), 7.20 (s, 2H, Ar), -3.25 (s, br, 1H, eq. ring CH₂), -5.38 (s, br, 1H, eq. ring CH₂), -5.78 (s, br, 1H, ax. ring CH₂), -8.70 (s, br, 1H, NCH₂CO), -9.63 (s, br, 1H, NCH₂CO); δ_C{¹H} (CD₃CN, 293 K) 194.6 (1C, CO), 134.9 (1C, Ar), 130.2 (2C, Ar), 128.4 (1C, Ar), 122.9 (2C, Ar), 100.4 (br, 1C, ring CH₂), 91.7 (br, 1C, ring CH₂), 82.8 (br, 1C, NCH₂CO). ν_{max} 3286 (NH), 1630 cm⁻¹ (C=O).

[Tb(L²)](CF₃SO₃)₃. Found: C, 38.80; H, 3.80; N, 8.39. Calc. for C₄₃H₄₈F₉N₈O₁₃S₃Tb: C, 38.86; H, 3.79; N, 8.43%. ν_{max} 3287 (N–H), 1630 cm⁻¹ (C=O).

[Sm(L³)(CH₃OH)](CF₃SO₃)₃·H₂O. Found: C, 34.17; H, 3.48; N, 11.07. Calc. for C₄₄H₅₀F₉N₁₂O₂₃S₃Sm: C, 34.49; H, 3.29; N, 10.97%. ν_{max} 3479 (OH), 3288 (NH), 1631 (C=O), 1530 and 1351 cm⁻¹ (NO₂).

[Eu(L³)(CH₃OH)](CF₃SO₃)₃·H₂O. Found: C, 34.14; H, 3.51; N, 11.05. Calc. for C₄₄H₅₀EuF₉N₁₂O₂₃S₃: C, 34.45; H, 3.29; N, 10.96%. δ_H (CD₃CN, 293 K) 19.75 (s, br, 1H, ax. ring CH₂), 8.36

(d, ²*J* = 7.5, 2H, Ar), 7.01 (d, ²*J* = 7.5 Hz, 2H, Ar), -2.89 (s, br, 1H, eq. ring CH₂), -4.52 (s, br, 1H, eq. ring CH₂), -7.12 (s, br, 1H, ax. ring CH₂), -8.65 (s, br, 1H, NCH₂CO), -9.79 (s, br, 1H, NCH₂CO); δ_C{¹H} (CD₃CN, 293 K) 192.1 (1C, CO), 145.4 (1C, Ar), 138.9 (1C, Ar), 124.1 (2C, Ar), 121.5 (2C, Ar), 103.4 (br, 1C, ring CH₂), 92.0 (br, 1C, ring CH₂), 80.6 (br, 1C, NCH₂CO). ν_{max} 3482 (OH), 3293 (NH), 1629 (C=O), 1530 and 1351 cm⁻¹ (NO₂).

[Tb(L³)(CH₃OH)](CF₃SO₃)₃·H₂O. Found: C, 34.10; H, 3.48; N, 11.05. Calc. for C₄₄H₅₀F₉N₁₂O₂₃S₃Tb: C, 34.45; H, 3.29; N, 10.96%. ν_{max} 3483 (OH), 3272 (NH), 1632 (C=O), 1530 and 1351 cm⁻¹ (NO₂).

[Lu(L³)]³⁺. δ_H (CD₃CN, 233 K, ESI, Fig. S5) 10.45 (s, br, 1H, NH), 8.24 (d, ²*J* = 9.1, 2H, Ar), 7.83 (d, ²*J* = 9.1, 2H, Ar), 3.96 (d, ²*J* = 18.2, 1H, NCH₂CO), 3.88 (d, ²*J* = 18.2, 1H, NCH₂CO), 3.50 (t, 1H, ²*J*_{gem(ax-eq)} = ³*J*_{ax-eq} = 14.1, ax. ring CH₂), 3.00 (d, 1H, ²*J*_{gem(ax-eq)} = 14.1, eq. ring CH₂), 2.80 (t, 1H, ²*J*_{gem(ax-eq)} = ³*J*_{ax-eq} = 14.1, ax. ring CH₂), 2.74 (d, 1H, ²*J*_{gem(ax-eq)} = 14.1, eq. ring CH₂). Note: the triplets are in fact triplets of doublets and the doublets, doublets of doublets, but the ³*J*_{ax-eq} coupling constant could not be determined. δ_C{¹H} (CD₃CN, 293 K) 175.9 (1C, CO), 144.6 (1C, Ar), 141.0 (1C, Ar), 124.7 (2C, Ar), 120.7 (2C, Ar), 55.5 (1C, ring CH₂), 54.6 (1C, ring CH₂), 63.4 (1C, NCH₂CO).

[Eu(L⁴)(CH₃OH)](CF₃SO₃)₃·H₂O. Found: C, 36.05; H, 3.77; N, 10.65. Calc. for C₄₈H₅₆EuF₉N₁₂O₂₂NS₃: C, 36.26; H, 3.68; N, 10.57%. ν_{max} 3430 (OH), 3293 (NH), 1630 (C=O), 1522 and 1350 cm⁻¹ (NO₂).

[Tb(L⁴)(CH₃OH)](CF₃SO₃)₃·2H₂O. Found: C, 35.07; H, 3.63; N, 10.34. Calc. for C₄₈H₆₀F₉N₁₂O₂₄S₃Tb: C, 35.69; H, 3.74; N, 10.41%. ν_{max} 3437 (OH), 3284 (NH), 1630 (C=O), 1520 and 1351 cm⁻¹ (NO₂).

Physico-chemical measurements

¹H and ¹³C NMR spectra were recorded on a Bruker AM-360 spectrometer (360.16 and 90.6 MHz, respectively) or on a Bruker Avance DRX-400 spectrometer (400.03 and 100.04 MHz). Proton chemical shifts are reported in parts per million (ppm) with respect to TMS, and ¹³C chemical shifts are related to CD₃CN (δ 0.3, 117.5). UV-VIS Electronic spectra were recorded at 293 K on a Perkin-Elmer Lambda 900 spectrometer, infrared spectra on a FT-IR Mattson Alpha Centauri spectrometer (4000–400 cm⁻¹, KBr pellets). Low-resolution luminescence measurements (spectra and lifetimes) were made on a Perkin-Elmer LS-50B spectrofluorimeter. High-resolution spectra and lifetimes after direct excitation of the metal ion were measured on a previously described instrumental set-up;⁴⁵ lifetimes are averages of at least four determinations. Quantum yields were determined in anhydrous and degassed MeCN with the help of a Perkin-Elmer LS-50B spectrofluorimeter relatively to EuL¹ for the europium complexes, and to a solution of quinine sulfate in 0.5 M H₂SO₄ (Φ_{abs} = 0.546) for terbium complexes by using eqn. (1) where *x* refers to the compound,

$$\frac{\Phi_x}{\Phi_r} = \frac{A_r(\lambda_r)I_r(\lambda_r)n_r^2D_x}{A_x(\lambda_x)I_x(\lambda_x)n_x^2D_r} \quad (1)$$

r to the reference, *A_r(λ_r)* is the absorbance at the excitation wavelength, *I* the intensity of excitation at λ_{*i*}, *n* the refractive index (*n*(CH₃CN) = 1.343, *n*(0.5 M H₂SO₄ in water) = 1.338), and *D* the area of the emission spectrum.⁴⁶

X-Ray crystallography

Single crystals of [Eu(L²)(H₂O)](CF₃SO₃)₃·4H₂O, [Eu(L³)(CH₃OH)](CF₃SO₃)₃·2CH₃OH and [Lu(L³)(CH₃OH)](Lu(L³)(H₂O)](CF₃SO₃)₆·10CH₃OH were obtained from acetonitrile-*tert*-butyl methyl ether for the former and methanol for the L³ complexes, and mounted in glass capillaries. Crystal data and

Table 6 Crystal data and structure refinement for: [Eu(L²)(H₂O)](CF₃SO₃)₃·4H₂O, [Eu(L³)CH₃OH][CF₃SO₃]₃·2CH₃OH, and [Lu(L³)-(CH₃OH)][Lu(L³)(H₂O)][CF₃SO₃]₆·10CH₃OH

	EuL ²	EuL ³	LuL ³
Formula	C ₄₃ H ₅₈ EuF ₉ N ₈ O ₁₈ S ₃	C ₄₆ H ₅₆ EuF ₉ N ₁₂ O ₂₄ S ₃	C ₉₇ H ₁₃₄ F ₁₈ Lu ₂ N ₂₄ O ₃₄ S ₆
<i>M</i>	1394.11	1580.17	3384.58
Crystal system	Monoclinic	Triclinic	Monoclinic
Space group	<i>I</i> 2/ <i>a</i>	<i>P</i> $\bar{1}$	<i>P</i> 2 ₁ / <i>n</i>
<i>a</i> /Å	21.556(4)	12.897(2)	13.239(3)
<i>b</i> /Å	23.387(5)	12.942(5)	35.095(7)
<i>c</i> /Å	23.239(5)	19.237(3)	29.656(6)
<i>a</i> ^o		87.85(3)	
<i>β</i> ^o	92.58(3)	84.358(10)	91.13(3)
<i>γ</i> ^o		86.51(3)	
<i>V</i> /Å ³	11704(4)	3187.8(14)	13776(5)
<i>Z</i>	8	2	4
<i>μ</i> /mm ⁻¹	0.600	1.194	1.636
Reflections collected	34295	17821	32581
Unique reflections	9529	10739	8387
[<i>I</i> > 2σ(<i>I</i>)]			
<i>R</i> [<i>I</i> > 2σ(<i>I</i>)]	0.0656	0.1055	0.0929
w <i>R</i> 2 (all data)	0.2097	0.2917	0.2781

structure refinement details are listed in Table 6. Diffraction data have been collected on a mar345 Imaging Plate Detector System at 143 K. Refinement of cell parameters, integration and scaling of data was performed with marHKL release 1.9.1.⁴⁷ No absorption correction was applied to any data set. Structures were solved by *ab initio* direct methods.⁴⁸ All structures were refined using full-matrix least squares on *F*² (except [Lu(L³)(CH₃OH)][Lu(L³)(H₂O)][CF₃SO₃]₆·10CH₃OH for which full-matrix-block least squares on *F*² was used) with all non-H atoms anisotropically defined. Some disorder problems arose during the refinement of [Eu(L²)(H₂O)][CF₃SO₃]₃·4H₂O and [Lu(L³)(CH₃OH)][Lu(L³)(H₂O)][CF₃SO₃]₆·10CH₃OH and they mostly dealt with CF₃SO₃⁻ anions for which some geometrical and rigid bond restraints were applied. Hydrogen atoms were placed in calculated positions using the riding model with a common isotropic displacement parameter (*U*_{iso} = 0.08 Å²). Space group determination, structure solution, refinement, molecular graphics and geometrical calculation have been carried out with the SHELXTL software package, release 5.1.⁴⁹ Selected bond lengths and angles are reported in Table S1 (ESI).

CCDC reference numbers 158148–158150.

See <http://www.rsc.org/suppdata/dt/b1/b101312m/> for crystallographic data in CIF or other electronic format.

Acknowledgements

This research is supported by grants from the Swiss National Science Foundation and the Swiss Federal Office for Science and Education (COST project D18). We thank the Fondation Herbette (Lausanne) for spectroscopic equipment and Dr P.-A. Pittet for synthesizing a first batch of ligands L² and L³.

References

- J.-C. G. Bünzli, N. André, M. Elhabiri, G. Muller and C. Piguet, *J. Alloys Compd.*, 2000, **303**–**304**, 66.
- X. Wang, T. Jin, V. Comblin, A. Lopez-Mut, E. Merciny and J.-F. Desreux, *Inorg. Chem.*, 1992, **31**, 1095.
- A. D. Sherry, C. R. Malloy, F. M. H. Jeffrey, W. P. Cacheris and C. F. G. C. Geraldès, *J. Magn. Reson.*, 1988, **76**, 528.
- P. Caravan, J. J. Ellison, J. M. Murry and R. B. Lauffer, *Chem. Rev.*, 1999, **9**, 2293.
- R. B. Lauffer, *MRI Clinical Magnetic Resonance Imaging*, eds R. E. Edelman, M. B. Zlatkin and J. R. Hesselink, W. B. Saunders Co, Philadelphia, 1996, vol. 1.
- S. Aime, M. Botta, S. G. Crich, E. Terreno, P. L. Anelli and F. Uggeri, *Chem. Eur. J.*, 1999, **5**, 1253.

- D. E. Reichert, J. S. Lewis and C. J. Anderson, *Coord. Chem. Rev.*, 1999, **184**, 3.
- J. Byegård, G. Skarnemark and M. Skålberg, *J. Radioanal. Nucl. Chem.*, 1999, **241**, 281.
- M. Komiyama, N. Takeda and H. Shigekawa, *Chem. Commun.*, 1999, 1443.
- D. M. Epstein, L. L. Chappell, H. Khalili, R. M. Supkowski, W. deW. Jr. Horrocks and J. R. Morrow, *Inorg. Chem.*, 2000, **39**, 2130.
- D. Parker, *Coord. Chem. Rev.*, 2000, **205**, 109.
- M. R. Spirlet, J. Rebizant, J. F. Desreux and M. F. Loncin, *Inorg. Chem.*, 1984, **23**, 359.
- J. A. K. Howard, A. M. Kenwright, J. M. Moloney, D. Parker, M. Port, M. Navet, O. Rousseau and M. Woods, *Chem. Commun.*, 1998, 1381.
- F. Benetollo, G. Bombieri, S. Aime and M. Botta, *Acta Crystallogr., Sect. C*, 1999, **55**, 353.
- S. Aime, A. S. Batsanov, M. Botta, J. A. K. Howard, M. P. Lowe and D. Parker, *New J. Chem.*, 1999, **23**, 669.
- S. Aime, A. S. Batsanov, M. Botta, J. A. K. Howard, D. Parker, K. Senanayake and J. A. G. Williams, *Inorg. Chem.*, 1994, **33**, 4696.
- S. Aime, A. S. Batsanov, M. Botta, R. S. Dickins, S. Faulkner, C. E. Foster, A. Harrison, J. A. K. Howard, J. M. Moloney, T. J. Norman, D. Parker, L. Royle and J. A. G. Williams, *J. Chem. Soc., Dalton Trans.*, 1997, 3623.
- J. Rohovec, P. Vojtišek, P. Hermann, J. Ludvík and I. Lukeš, *J. Chem. Soc., Dalton Trans.*, 2000, 141.
- J. R. Morrow, S. Amin, C. H. Lake and M. R. Churchill, *Inorg. Chem.*, 1993, **32**, 4566.
- S. Amin, J. R. Morrow, C. H. Lake and M. R. Churchill, *Angew. Chem., Int. Ed. Engl.*, 1994, **33**, 773.
- S. Amin, D. A. Voss, W. deW. Jr. Horrocks, C. H. Lake, M. R. Churchill and J. R. Morrow, *Inorg. Chem.*, 1995, **34**, 3294.
- R. S. Dickins, J. A. K. Howard, C. W. Lehmann, J. Moloney, D. Parker and R. D. Peacock, *Angew. Chem., Int. Ed. Engl.*, 1997, **38**, 521.
- R. S. Dickins, J. A. K. Howard, C. L. Maupin, J. M. Moloney, D. Parker, J. P. Riehl, G. Siligardi and J. A. G. Williams, *Chem. Eur. J.*, 1999, **5**, 1095.
- S. Aime, A. Barge, J. I. Bruce, M. Botta, J. A. K. Howard, J. M. Moloney, D. Parker, A. S. de Sousa and M. Woods, *J. Am. Chem. Soc.*, 1999, **121**, 5762.
- G. Zucchi, R. Scopelliti, P.-A. Pittet, J.-C. G. Bünzli and R. D. Rogers, *J. Chem. Soc., Dalton Trans.*, 1999, 931.
- L. Alderighi, A. Bianchi, L. Calabi, P. Dapporto, C. Giorgi, P. Losi, L. Paleari, P. Paoli, P. Rossi, B. Valtancoli and M. Virtuani, *Eur. J. Inorg. Chem.*, 1998, 1581.
- J. Dale, *Isr. J. Chem.*, 1980, **20**, 3.
- J. P. Dubost, J. M. Leger, M.-H. Langlois, D. Meyer and M. Schaefer, *C. R. Acad. Sci.*, 1991, **312**, 349.
- D. Parker, K. Pulukkody, F. C. Smith, A. Batsanov and J. A. K. Howard, *J. Chem. Soc., Dalton Trans.*, 1994, 689.
- S. Aime, A. Barge, M. Botta, M. Fasano, J. D. Ayala and G. Bombieri, *Inorg. Chim. Acta*, 1996, **246**, 423.
- G. Bombieri, *J. Alloys Compd.*, 1997, **249**, 76.

- 32 K. O. A. Chin, J. R. Morrow, C. H. Lake and M. R. Churchill, *Inorg. Chem.*, 1994, **33**, 656.
- 33 S. T. Frey and W. deW. Horrocks Jr., *Inorg. Chim. Acta*, 1995, **229**, 383.
- 34 G. Zucchi, PhD Dissertation, University of Lausanne, 2000.
- 35 S. Aime, M. Botta and G. Ermondi, *Inorg. Chem.*, 1992, **31**, 4291.
- 36 F. A. Dunand, S. Aime and A. E. Merbach, *J. Am. Chem. Soc.*, 2000, **122**, 1506.
- 37 C. Platas, F. Avecilla, A. de Blas, C. F. G. C. Geraldes, T. Rodriguez-Blas, H. Adams and J. Mahia, *Inorg. Chem.*, 1999, **38**, 3190.
- 38 T. Förster, *Ann. Phys. (Leipzig)*, 1948, **2**, 55.
- 39 A. Beeby, I. M. Clarkson, R. S. Dickins, S. Faulkner, D. Parker, L. Royle, A. S. de Sousa, J. A. G. Williams and M. Woods, *J. Chem. Soc., Perkin Trans. 2*, 1999, 493.
- 40 H.-R. Mürner, E. Chassat, R. P. Thummel and J.-C. G. Bünzli, *J. Chem. Soc., Dalton Trans.*, 2000, 2809.
- 41 D. D. Perrin and W. L. F. Armarego, *Purification of Laboratory Chemicals*, Pergamon Press, Oxford, 1988.
- 42 J.-C. G. Bünzli and F. Pilloud, *Inorg. Chem.*, 1989, **28**, 2638.
- 43 P. A. Pittet, D. Früh, V. Tissières and J.-C. G. Bünzli, *J. Chem. Soc., Dalton Trans.*, 1997, 895.
- 44 T. Hamada, Y. Okuno, M. Ohmori, T. Niski and O. Yonemitsu, *Chem. Pharm. Bull.*, 1981, **29**, 128.
- 45 J.-C. G. Bünzli and A. Milicic-Tang, *Inorg. Chim. Acta*, 1996, **252**, 221.
- 46 S. Petoud, J.-C. G. Bünzli, K. J. Schenk and C. Piguet, *Inorg. Chem.*, 1997, **36**, 1345.
- 47 Z. Otwinowski and W. Minor, *Methods Enzymol.: Macromolecular Crystallogr.*, 1997, **276**, 307.
- 48 G. M. Sheldrick, *Acta Crystallogr., Sect. A*, 1990, **46**, 467.
- 49 SHELXTL, I. Bruker AXS, Madison, WI, 1997.